

NUMERICAL STUDY OF FLOW AND HEAT TRANSFER IN DIFFERENTIALLY HEATED ENCLOSURES

by

Byong-Hoon CHANG

School of Mechanical System Engineering, Incheon National University, Incheon, South Korea

Original scientific paper
DOI: 10.2298/TSCI110626007C

Two-dimensional laminar natural convection is studied numerically for differentially heated air-filled rectangular enclosures with adiabatic side walls and aspect ratios of 1, 2, 4, and 8. The inclination angle of the enclosure was varied from 0° to 180°, and the effect of inclination on flow field and heat transfer was investigated over the range $10^3 \leq Ra \leq 10^6$. Correlations of average Nusselt number based on the present results are presented for horizontal and vertical cases. Large discrepancies were found among published results.

Key words: *natural convection, rectangular enclosure, aspect ratio, inclination*

Introduction

Natural convection in rectangular enclosures has been studied extensively, but there have been relatively few studies investigating both the effects of inclination angle and aspect ratio on flow and heat transfer. The effect of inclination angle on heat transfer was first studied by Dropkin and Somerscales [1] who used water, silicone oil, and mercury in rectangular enclosure of aspect ratios between 3.5 and 14. Their experiment was performed for $5 \cdot 10^4 \leq Ra \leq 7.17 \cdot 10^8$, and $0^\circ \leq \theta \leq 90^\circ$. Five Nusselt number correlations were given for each respective inclination angle, but the effect of aspect ratio (AR) was not included unlike other experimental results from vertical layers [2, 3]. Arnold *et al.* [4] investigated the effects of inclination angle using water and silicone oil in rectangular enclosures with $1 \leq AR \leq 12$, $10^3 \leq Ra \leq 10^6$, and $0^\circ \leq \theta \leq 180^\circ$. Correlations use the given Nusselt numbers at $\theta = 0^\circ$ and 90° to predict Nusselt number at other inclination angle, but the effect of aspect ratio was not considered. Ozoe *et al.* [5] used air in rectangular enclosures of $AR = 8.4$ and 15.5 , and silicone oil in rectangular enclosures of $AR = 1, 2, 3$, and 4.2 , for the range $3 \cdot 10^3 \leq Ra \leq 10^5$. For silicone oil, the following form of the Nusselt number correlation was proposed, and 5 or 6 different sets of the coefficients A and B were given for each aspect ratio at various inclination angles. A total of 21 sets of coefficients were presented:

$$\overline{Nu} = A \cdot Ra^B \quad (1)$$

Inaba [6] performed experiments for an air layer of $5 \leq AR \leq 83$, $0^\circ \leq \theta \leq 180^\circ$ and $1.2 \cdot 10^3 \leq Ra \leq 2 \cdot 10^6$. For inclination angles of $0^\circ \leq \theta \leq 60^\circ$, the average Nusselt number appeared fairly insen-

* Authors' e-mail: bhchang@incheon.ac.kr

sitive to the change in aspect ratio, but some data were not in the same range of Ra. More investigation seems needed for smaller aspect ratio range. Hamady *et al.* [7] studied the effect of inclination angle for air in rectangular enclosure of $AR = 1$ for Rayleigh number between 10^3 and 10^6 both experimentally and numerically. Over-estimation of Nusselt number from the adiabatic boundary condition compared to the experimental condition was discussed. Visualization of flow patterns and isotherms were presented, but a Nusselt number correlation was proposed for $\theta = 90^\circ$ only. Flow mode transition from inclination was studied numerically for the aspect ratio of 4 by Soong *et al.* [8]. Hysteresis phenomena showing dual solutions were found to exist as the computation was performed by increasing or decreasing the inclination angle. The effect of initial temperature field and imperfect thermal boundary condition were examined for $AR = 1$ and 3, but Nusselt number correlation was not given. Effects of six different thermal boundary conditions of the vertical sidewalls on flow field and heat transfer were studied numerically for air, for the range of $0.66 \leq AR \leq 8$, $10^4 \leq Ra \leq 10^6$ by Corcione [9]. Various Nusselt number correlations were given for bottom, top and side walls for each thermal boundary condition, but only for horizontal cases. Wang and Hamed [10] performed a numerical study for an air-filled rectangular enclosure of $AR = 4$ over the range of $10^3 \leq Ra \leq 10^4$ and $0^\circ \leq \theta \leq 90^\circ$. Effects of four thermal boundary conditions on the sidewalls and hysteresis phenomena were investigated, but Nusselt number correlation was not given. Both experimental and numerical study were performed by Bairi *et al.* [11] for air layer of $AR = 0.67$ and 1.33 for $10 \leq Ra \leq 10^8$ and $0^\circ \leq \theta \leq 360^\circ$. Four Nusselt number correlations were given at various inclination angles, and it was concluded that 3-D effects at the edge are small and the 2-D model is suitable. But their comparison with published data is confusing – De Vahl Davis' data [12] of 90° seem to have been compared with their 0° data (which is 90° in their notation). Previous numerical works in enclosed enclosures include studies on various aspects such as thermal boundary conditions, hysteresis phenomena and inclination angles, but there is no work done on the effect of inclination on flow field and heat transfer over larger range of aspect ratio, as in the present study. Furthermore, there are wide disagreements among correlations and lack of information even for simpler configurations of horizontal or vertical layers, as will be shown later. Relevant and practical studies can be found in literature [13-16].

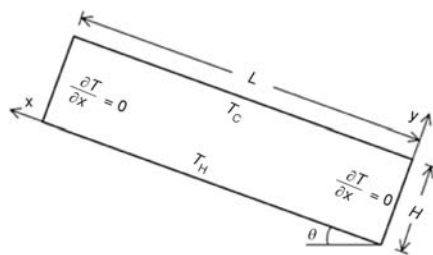


Figure 1. Schematic of the computational domain

Analysis

Figure 1 shows the geometry of the present numerical study. The bottom and the top of the rectangular enclosure are kept at constant temperatures T_H and T_C , respectively, and are separated by height H . The other two facing sidewalls are adiabatic as indicated in fig. 1. For the computational domain, a power-law grid was used with higher density near the walls. Governing equations for steady 2-D laminar flow with constant properties and Boussinesq approximation are as:

$$\frac{\partial u}{\partial x} = \frac{\partial v}{\partial y} = 0 \quad (2)$$

$$u \frac{\partial u}{\partial x} + v \frac{\partial u}{\partial y} = -\frac{1}{\rho} \frac{\partial p}{\partial x} + \nu \nabla^2 u + g\beta(T - T_0) \sin \theta \quad (3)$$

$$u \frac{\partial v}{\partial x} + v \frac{\partial v}{\partial y} = -\frac{1}{\rho} \frac{\partial p}{\partial y} + \nu \nabla^2 v + g\beta(T - T_0) \cos \theta \quad (4)$$

$$u \frac{\partial T}{\partial x} + v \frac{\partial T}{\partial y} = \alpha \nabla^2 T \quad (5)$$

The discretized equations were solved using PHOENICS [17]. But, the buoyancy terms were coded separately into PHOENICS, and the provided method in PHOENICS was not used. The pressure-velocity coupling in PHOENICS is solved by the SIMPLEST [18] algorithm in which coefficients for the momentum equations contain only diffusion contributions and the convection terms are added to the linearized source terms. The convective terms were approximated by the hybrid scheme in almost all cases, but Van Leer' [19] second order scheme and the SMART scheme of Gaskell and Lau [20] were also used to remove numerical oscillations in some cases, as discussed in the next section. The sum of the absolute value of the residuals for each variable, the change of local values at a specific location, and finally the average Nusselt number were monitored with iteration. The relative change of the velocities, pressure and temperature were all less than 10^{-5} when solution was regarded as converged. At low Ra, the relative change in Nu was practically zero, and less than 10^{-5} even near flow-mode transition to a uni-cell where a sudden drop in heat transfer occurred. But, convergence was more difficult to achieve for $Ra = 10^6$, and near the flow-mode transition to a uni-cell. There were very small fluctuations in the average Nusselt number, but the relative change was about $4 \cdot 10^{-4}$ for $AR = 8$ near the flow-mode transition to a unicell. The average Nusselt number was calculated as:

$$\overline{Nu} = -\frac{1}{L} \int_0^L \frac{H}{\Delta T} \frac{\partial T}{\partial y} \Big|_{y=0} dx \quad (6)$$

Results and discussion

A square cavity with differentially heated sidewalls and adiabatic top and bottom walls was solved first in order to validate the code. As with Barakos *et al.* [21], the temperature difference was kept at 20 °C and the reference temperature was 20 °C. The cavity dimension was increased to obtain higher Ra, and the same dimensions of Barakos *et al.* [21] were used. Figure 2 shows the computed results of velocity field, streamlines, and isotherms for $Ra = 10^3$, 10^4 , 10^5 , and 10^6 . Computed average Nusselt number, the maximum and minimum Nusselt numbers and

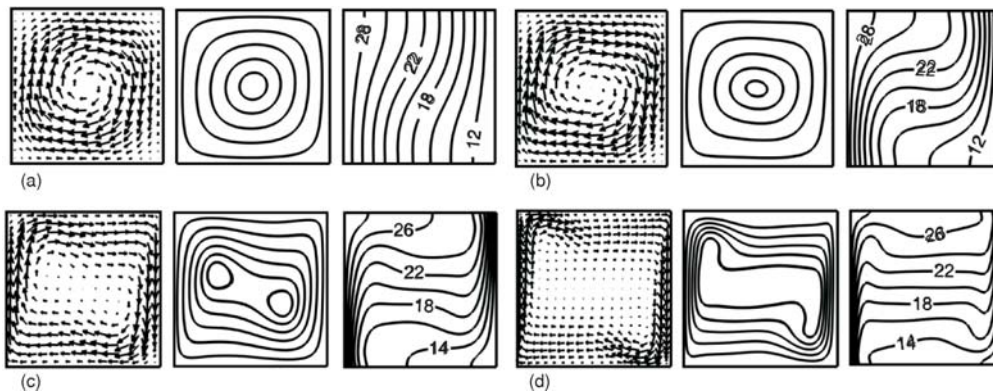


Figure 2. Calculated velocities, streamlines, and isotherms for Ra of (a) 10^3 , (b) 10^4 , (c) 10^5 , and (d) 10^6

velocities, and their locations are listed in tab. 1. 2-D [12, 21, 22] and 3-D results [23] in literature are also summarized for comparison. Present results are all very close to those of De Vahl Davis [12] except the value of u_{\max} at $Ra = 10^5$ which is about 15.7% lower. However, other published results [21, 22] also show 13.7~14.4% lower u_{\max} at $Ra = 10^5$. The difference in the average Nusselt number between 60×60 grid and 80×80 grid was about 0.2%, and the present results in tab. 1. were all obtained with 80×80 non-uniform grid. Figure 3 shows comparison of present field variables with the experimental data of Krane and Jessee [24] for $Ra = 1.89 \cdot 10^5$. Current results in fig. 3 show a fairly good agreement with experimental data, except for some under-prediction of the velocity maxima.

Table 1. Comparison of laminar solution with previous results

	Present study	Khanafer <i>et al.</i> [22]	Barakos <i>et al.</i> [21]	De Vahl [12]	Fusegi <i>et al.</i> [23]
$Ra = 10^3$					
\overline{Nu}	1.118	1.118	1.114	1.118	1.105
Nu_{\max} (at y/H)	1.506(0.087)		1.581(0.099)	1.505(0.092)	1.420(0.083)
Nu_{\min} (at y/H)	0.691(1.0)		0.670(0.994)	0.692(1.0)	0.764(1.0)
u_{\max} (at y/H)	0.137 (0.813)	0.137 (0.812)	0.153(0.806)	0.136(0.813)	0.131(0.8)
v_{\max} (at x/L)	0.139 (0.178)	0.139 (0.173)	0.155(0.181)	0.138(0.178)	0.132(0.167)
$Ra = 10^4$					
\overline{Nu}	2.241	2.245	2.245	2.243	2.302
Nu_{\max} (at y/H)	3.529(0.144)		3.539(0.143)	3.528(0.143)	3.652(0.623)
Nu_{\min} (at y/H)	0.582(1.0)		0.583(0.994)	0.586(1.0)	0.611(1.0)
u_{\max} (at y/H)	0.192 (0.823)	0.192 (0.827)	0.193 (0.818)	0.192 (0.823)	0.201(0.817)
v_{\max} (at x/L)	0.234 (0.119)	0.233 (0.123)	0.234 (0.119))	0.234 (0.119)	0.225(0.117)
$Ra = 10^5$					
\overline{Nu}	4.532	4.522	4.510	4.519	4.646
Nu_{\max} (at y/H)	7.748(0.0813)		7.636(0.085)	7.717(0.081)	7.795(0.0826)
Nu_{\min} (at y/H)	0.726(1.0)		0.773(0.999)	0.729(1.0)	0.787(1.0)
u_{\max} (at y/H)	0.129 (0.853)	0.131 (0.854)	0.132 (0.859)	0.153 (0.855)	0.147(0.855)
v_{\max} (at x/L)	0.259 (0.0654)	0.258 (0.065)	0.258 (0.066)	0.261 (0.066)	0.247(0.065)
$Ra = 10^6$					
\overline{Nu}	8.848	8.826	8.806	8.799	9.012
Nu_{\max} (at y/H)	17.709(0.0372)		17.442(0.0368)	17.925(0.0378)	17.670(0.0379)
Nu_{\min} (at y/H)	0.985(1.0)		1.001(0.999)	0.989(1.0)	1.257(1.0)
u_{\max} (at y/H)	0.077 (0.847)	0.077 (0.854)	0.077 (0.859)	0.079 (0.850)	0.084(0.856)
v_{\max} (at x/L)	0.263 (0.0373)	0.262 (0.039)	0.262 (0.039)	0.262 (0.038)	0.259(0.033)

For computations of all configuration, the $\theta = 0^\circ$ case was computed first, and its velocity and temperature fields were used as initial conditions for subsequent inclination. The inclination angle was increased by 5° or 10° , but was increased by 1° near flow mode transition where there may be a sudden change in heat transfer. Figure 4 shows computed results at various inclination angles for $AR = 1$ and $Ra = 10^5$. Small recirculating cells in the lower right hand corner and in the upper left hand corner in fig. 4(a) become much larger at $\theta = 15^\circ$ in fig. 4(b). It can be seen in fig. 5 that the growth of these secondary cells is accompanied by decline in overall

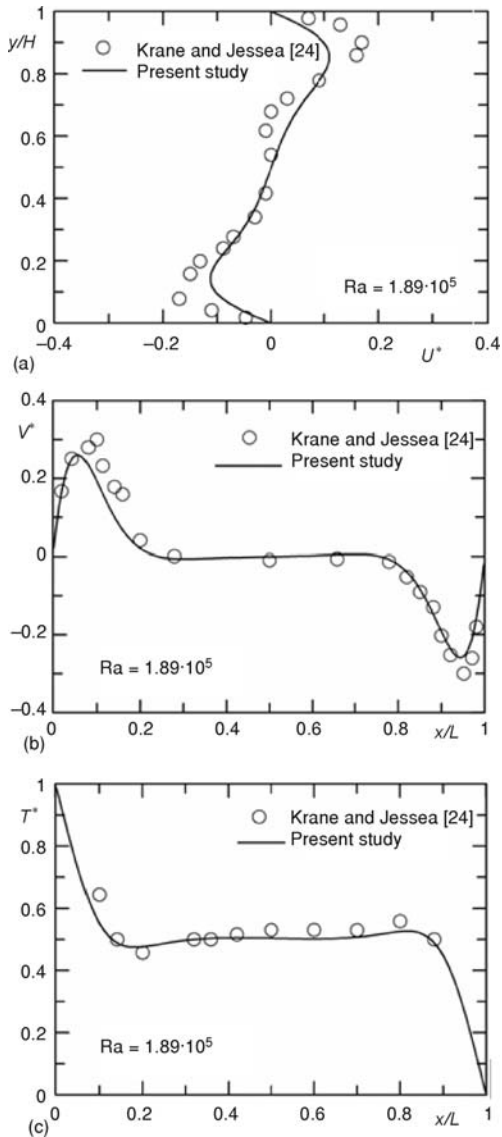


Figure 3. Comparison of present results with experimental data of Krane and Jessee [24]

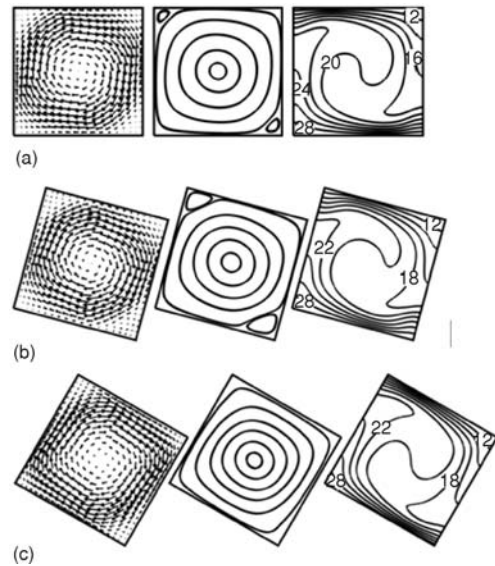


Figure 4. Calculated velocities, streamlines, and isotherms for $AR = 1$, $Ra = 10^5$, and (a) $\theta = 0^\circ$, (b) $\theta = 15^\circ$, (c) $\theta = 30^\circ$

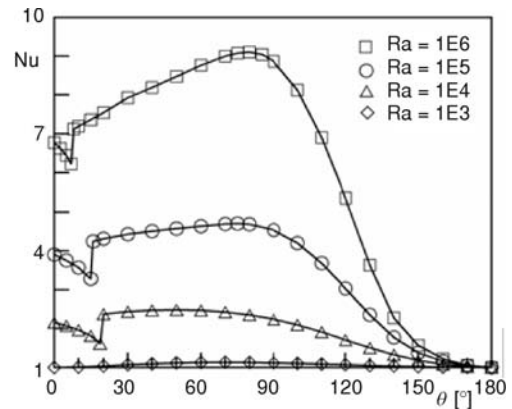


Figure 5. Calculated average Nusselt numbers for $AR = 1$

heat transfer. As the inclination angle is increased further, these cells in the corner disappear and fig. 5 shows a sudden increase in heat transfer. At $\theta = 90^\circ$ vertical walls are isothermal, and two co-rotating cells are formed in the center streamline as in fig. 2(c). The velocity field was not plotted at all grid points for clarity.

Hamady *et al.* [7] and Kuyper *et al.* [25] investigated the effect of inclination on heat transfer for $AR = 1$ numerically. Their initial computation was performed for $\theta = 180^\circ$ at which the hot wall is at the top, and the inclination angle was decreased for subsequent calculations.

3-D calculations for $Ra = 1.1 \cdot 10^5$ using the QUICK scheme by Hamady *et al.* [7] became unstable below 30° , and convergence of 2-D calculation for $Ra = 10^6$ using central difference scheme by Kuyper *et al.* [25] was reported too slow for inclination angle below 20° , and further calculations were not considered. In the present calculation for $Ra = 10^6$, the initial computation at $\theta = 0^\circ$ using hybrid difference scheme (which is the same as the central difference scheme for absolute grid Peclet number less or equal to 2) was unstable. A steady-state solution for $\theta = 0^\circ$ could be obtained with Van Leer's second order, bounded TVD scheme [19] which is known to eliminate spurious numerical oscillations, and this scheme was used up to $\theta = 20^\circ$. The difference in average Nusselt number between Van Leer's scheme and the hybrid scheme was about 0.13% for $\theta = 20^\circ$. The SMART scheme of Gaskell and Lau [20] was also tested, and the difference in average Nusselt number between Van Leer's scheme and SMART scheme was 0.15% for $\theta = 0^\circ$.

Depending on whether computation is performed increasing or decreasing the inclination angle, transition between a multi-cell structure and a unicell structure was found to occur at a different inclination angle [8, 10], and the investigation about this hysteresis was not repeated in the present study. The average Nusselt number of Hamady *et al.* experimental data for $\theta = 90^\circ$ and $Ra = 8.7 \cdot 10^5$ [7] is about 7.8, and this value is about 11% lower than the benchmark value of De Vahl Davis [12]. However one study [26] shows that using the experimental boundary condition gives around 20% lower average Nusselt number than the numerical solution obtained with the adiabatic boundary condition in the range $10^5 \leq Ra \leq 10^6$. Thus, care must be taken when comparing with experimental results that had conduction near the end walls. Present results and numerical results of Kuyper *et al.* [25] for $Ra = 10^6$ are almost identical over the range $20^\circ \leq \theta \leq 180^\circ$.

The difference in the average Nusselt number between 34×68 grid and 50×100 grid for $AR = 2$ and $Ra = 10^6$ was about 0.05%, and 34×68 grid was used in all calculations of $AR = 2$ case. As the angle was increased from the $\theta = 0^\circ$ case of fig. 6(a) the lower cell starts to shrink, and a secondary flow formed in the upper right hand corner as can be seen in fig. 6(b). Figure 7 shows that heat transfer is the lowest at this inclination angle of 12.5° . Though not shown in fig. 6(d) of $\theta = 90^\circ$, there were two co-rotating cells in the center as in $\theta = 45^\circ$ case. Compared to the gradual flow transition for $Ra = 10^5$, two-cell to one-cell flow transition takes place at $\theta = 4^\circ$ in the case of $Ra = 10^6$, where a sudden drop in average Nusselt number can be seen in fig. 7. At 4° , two small secondary flows formed in the opposite corners in addition to the main re-circulating

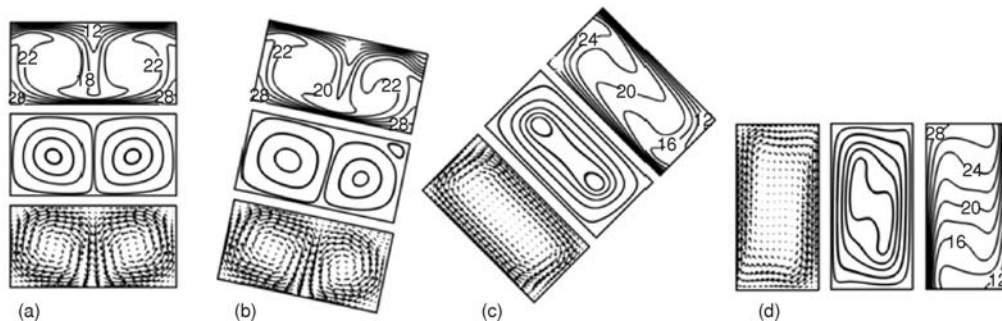


Figure 6. Calculated velocities, streamlines, and isotherms for $AR = 2$, $Ra = 10^5$, and (a) $\theta = 0^\circ$, (b) $\theta = 12.5^\circ$, (c) $\theta = 45^\circ$, and (d) $\theta = 90^\circ$

cell. But as the inclination angle is increased, these became weak and the boundary layer near the walls became thinner leading to increase in overall heat transfer.

Figure 8(a) shows a four-cell structure at $\theta = 0^\circ$ for a rectangular enclosure with $AR = 4$. The four-cell structure remained up to $\theta = 15^\circ$, and it changed to a three-cell structure of 1.96:1:1.86 size ratio at $\theta = 15.5^\circ$. The three-cell-structure persisted up to $\theta = 40^\circ$ as the upper cell increased 27% in size whereas the size of middle cell decreased 55%. The location where the average Nusselt number shows a sudden decrease in fig. 9 is where the three-cell structure changes to a single cell. Though not plotted in fig. 8(d) there was a weak tertiary flow in the middle of the enclosure at $\theta = 90^\circ$. Comparison was made with the numerical results of Soong *et al.* [8] to verify the accuracy of the current results, and fig. 10 shows a

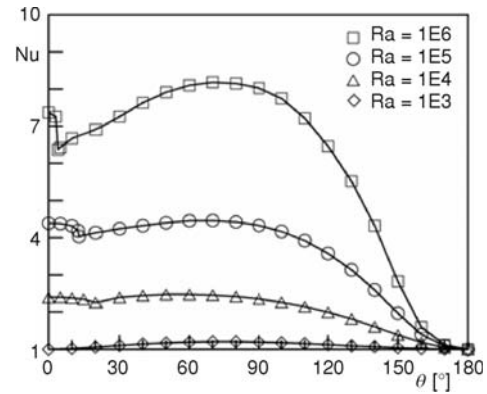


Figure 7. Calculated average Nusselt numbers for $AR = 2$

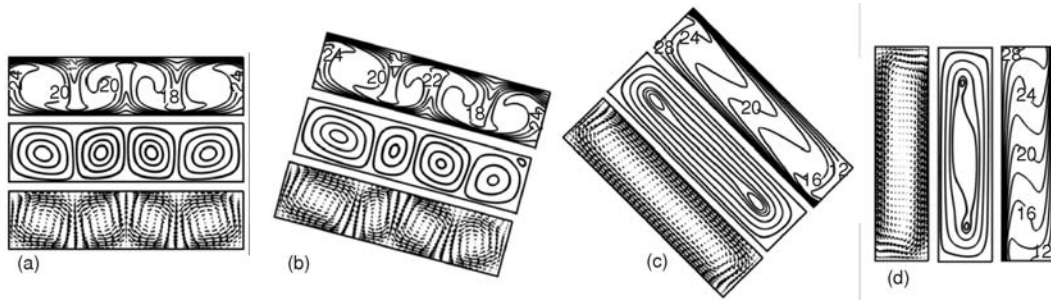


Figure 8. Calculated velocities, streamlines, and isotherms for $AR = 4$, $Ra = 10^5$, and (a) $\theta = 0^\circ$, (b) $\theta = 15^\circ$, (c) $\theta = 45^\circ$, and (d) $\theta = 90^\circ$

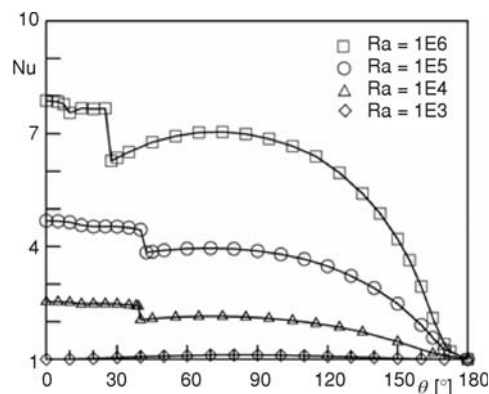


Figure 9. Calculated average Nusselt numbers for $AR = 4$

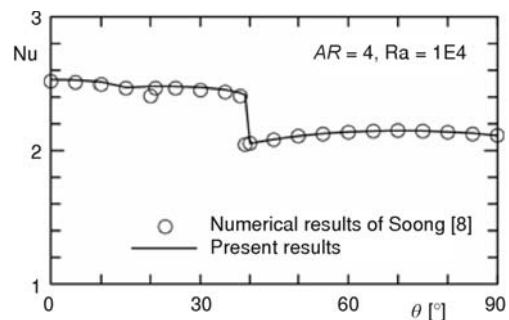


Figure 10. Comparison of average Nusselt number variation with Soong *et al.* [8]

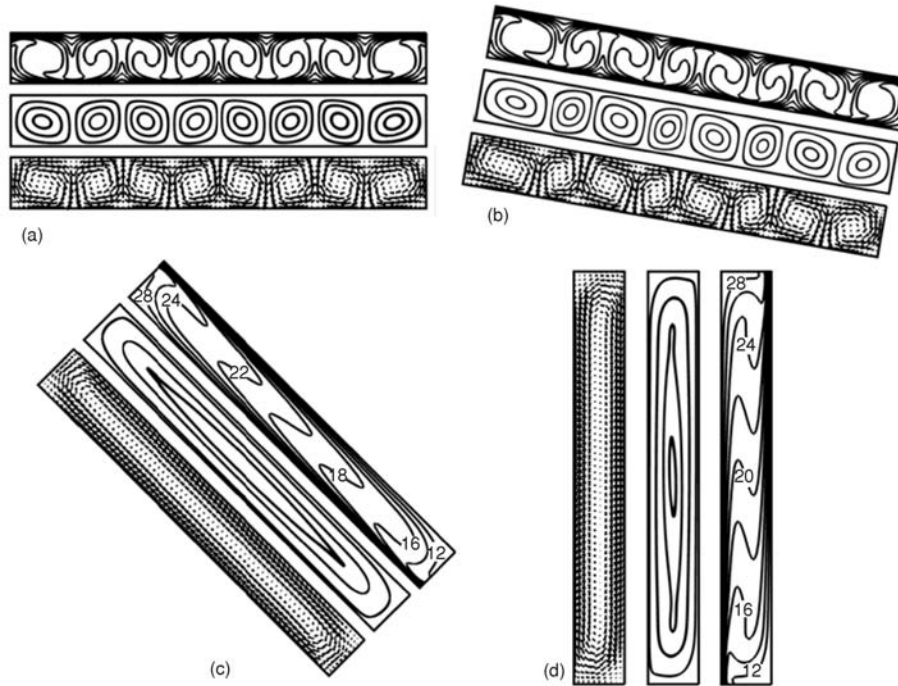


Figure 11. Calculated velocities, streamlines, and isotherms for $AR = 8$, $Ra = 10^5$, and (a) $\theta = 0^\circ$, (b) $\theta = 10^\circ$, (c) $\theta = 45^\circ$, and (d) $\theta = 90^\circ$

very close agreement. Figures 11 and 12 show similar results of flow field and average Nusselt number obtained with $AR = 8$. Inclination angles where flow mode transition takes place were very close to the $AR = 4$ case, but average Nusselt number for $AR = 8$ was lower for larger inclination angles due to decrease in heat transfer from growing thermal boundary layer thickness along the active walls. Local heat transfer rates along the hot wall for $AR = 1$ and 8 are plotted in fig. 13.

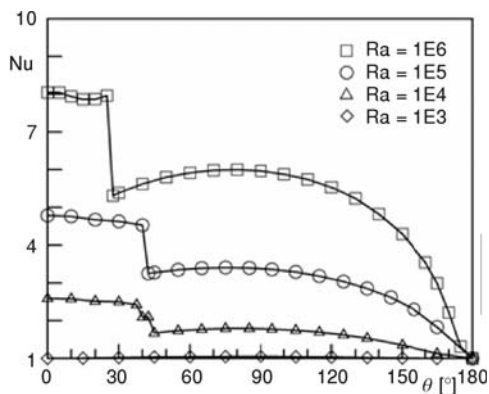


Figure 12. Calculated average Nusselt numbers for $AR = 8$

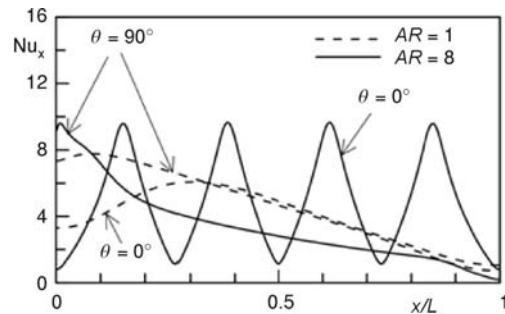


Figure 13. Nusselt number profiles for $Ra = 10^5$ at $\theta = 0^\circ$ and 90°

The inclination angles of the maximum and minimum heat transfer are plotted in fig. 14 for aspect ratios of 1, 2, 4, and 8. The maximum heat transfer occurs between 50° and 80° for the square enclosure, but the inclination angle of the maximum heat transfer approaches 0° with the increase of aspect ratio. The inclination angle of the minimum heat transfer in fig. 14 is the angle where flow-mode transition occurs with subsequent change in Nusselt number. It occurs between 7° and 19° for $AR = 1$, and its location increases about 20° as the aspect ratio approaches 4. The multi-cell structure changes to single cell at lower inclination angle for high Rayleigh number case, and this leads to minimum heat transfer at lower angles. As with the maximum heat transfer, the location of minimum heat transfer hardly changed from $AR = 4$ to $AR = 8$. Some published experimental results [4] claim that the secondary maximum heat transfer occurs at 90° for $AR = 1, 3, 6$ and 12. However, experimental results of Ozoe *et al.* [5] show that the secondary maximum occurs at angles less than 90° for $1 \leq AR \leq 15.5$, as the present results show in figs. 5, 7, 9, and 12.

Based on the present numerical results eqs. (7) and (8) are derived and comparison is made in fig. 15:

$$Nu = 0.189AR^{0.11}Ra^{0.26}, \quad \theta = 0^\circ \quad (7)$$

$$Nu = 0.223AR^{-0.11}Ra^{0.26}, \quad \theta = 90^\circ \quad (8)$$

Equation (7) predicts the present 0° data within ±7%, and eq. (8) predicts the present 90° data within ±9% for $10^4 \leq Ra \leq 10^6$. Other relevant published correlations for air layers are listed in tab. 2. The slope to Ra for $\theta = 0^\circ$ in eq. (7) is close to that of Inaba's correlation 0.258 [6]. For vertical layers of $\theta = 90^\circ$, the slope to Ra for $AR = 1$ was 0.299 for $AR = 1$, which is close to Berkovsky and Polevikov's 0.29 [27]. The correlations of Berkovsky and Polevikov [27] for $\theta = 90^\circ$ are $\overline{Nu} = 0.18[RaPr/(0.2 + Pr)]^{0.29}$ for $1 < AR < 2$, and $\overline{Nu} = 0.22[RaPr/(0.2 + Pr)]^{0.28}AR^{-0.25}$ for $2 < AR < 10$. They are recommended in some widely used textbooks [28, 29]. For other aspect ratios of the present study, the slopes to Ra were 0.267, 0.258, and 0.261 for $AR = 2, 4$, and 8, respectively. The slope of 0.26 in eq. (8) is the average of these values. This value is a bit lower than Berkovsky and Polevikov's 0.28 [27]. For $AR = 1$, a separate correlation with the exponent of 0.3 is more appropriate, but comparing the results with the correlations of Hamady *et al.* [7] and Berkovsky and Polevikov [27], eq. (8) was found quite adequate for $AR = 1$ also.

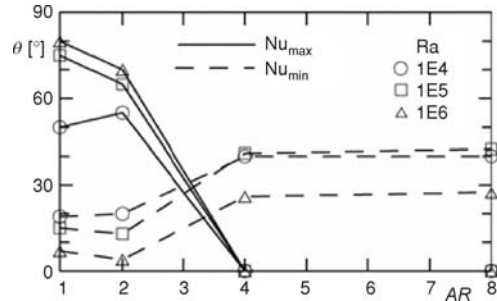


Figure 14. Effect of aspect ratio on the inclination angle of the maximum and minimum Nusselt numbers

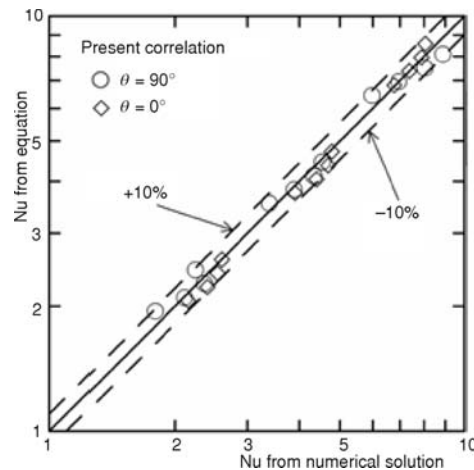


Figure 15. Comparison of Nusselt numbers predicted by eqs. (7) and (8) with the present numerical results

Table 2. Correlations of average Nusselt number for rectangular enclosures

Investigation	Method	Inclination angle	Aspect ratio	Range of Ra or Gr	Correlation of \overline{Nu}
Ozoe <i>et al.</i>	Exp.	Low angles	8.4, 15.5	$10^3 < Ra < 4 \cdot 10^4$	$0.10^9 Ra^{1/3} (\cos\theta)^{1/3}$
Inaba	Exp.	$0^\circ \leq \theta \leq 60^\circ$	$5 \leq AR \leq 83$	$6 \cdot 10^3 \leq Ra \cos\theta \leq 4 \cdot 10^5$	$0.199(Ra \cos\theta)^{0.258}$
Corcione	Num.	0°	$0.66 \leq AR \leq 8$	$5 \cdot 10^3 \leq Ra \sin\theta \leq 1.2 \cdot 10^6$	$0.21 Ra^{0.25} AR^{0.09}$
Bairi <i>et al.</i>	Exp, num.	0°	0.67, 1.33	$10^3 < Ra < 10^8$	$0.133 Ra^{0.304}$
Bairi <i>et al.</i>	Exp, num.	90°	"	"	$0.147 Ra^{0.287}$
Hamady	Exp, num.	90°	1	$10^3 < Ra < 10^6$	$0.175 Ra^{0.275}$
Jacob	Exp.	90°	$3.12 \leq AR \leq 42.2$	$2 \cdot 10^4 \leq Gr \leq 2 \cdot 10^5$	$0.18 Gr^{0.25} AR^{-0.111}$
Jacob	Exp.	"	"	$2 \cdot 10^5 \leq Gr \leq 2 \cdot 10^7$	$0.065 Gr^{0.333} AR^{-0.111}$
Inaba	Exp	$60^\circ \leq \theta \leq 120^\circ$	$5 \leq AR \leq 83$	$5 \cdot 10^3 \leq Ra \sin\theta \leq 1.2 \cdot 10^6$	$0.271 (Ra \sin\theta)^{0.25} AR^{-0.21}$
Yin <i>et al.</i>	Exp.	90°	$4.9 \leq AR \leq 78.7$	$1.5 \cdot 10^3 \leq Gr \leq 7 \cdot 10^6$	$0.21 Gr^{0.269} AR^{-0.131}$
Eckert <i>et al.</i>	Exp.	90°	10	$8 \cdot 10^4 \leq Gr \leq 2 \cdot 10^5$	$0.119 Gr^{0.3} AR^{-0.1}$
Newell <i>et al.</i>	Num.	90°	$2.5 \leq AR \leq 20$	$4 \cdot 10^4 \leq Gr \leq 1.4 \cdot 10^5$	$0.155 Gr^{0.315} AR^{-0.265}$

Figures 16 and 17 show comparisons of various Nusselt number correlations in tab. 2 in the range $10^4 \leq Ra \leq 10^5$ and for $AR = 8$ only, which is close to the valid range of correlations listed. Figure 16 shows that the current correlation compares fairly good with others except for Inaba's correlation [6]. The aspect ratios used to derive Inaba's correlation were mostly 5, 10, and 29, and Ozoe *et al.* [5] is based on $AR = 8.4$ and 15.5, and up to $Ra \approx 4 \cdot 10^4$. But, the difference between the two experimental correlations of air layers is 22% at $Ra = 4 \cdot 10^4$ and over 30% at $Ra = 10^5$ if correlation of Ozoe *et al.* is extrapolated. For horizontal layer of air, only correlations for large aspect ratio are given in textbooks [28, 29], namely $AR \geq 12$. For $\theta = 90^\circ$, fig. 17 shows that values given by eq. (8) lie between those of Yin *et al.* [30] and Eckert and Carlson [31]. Inaba's [6] correlation lie between Eckert and Carlson [31] and Berkovsky and Polevikov [27], except for $Ra < 2 \cdot 10^4$. The exponent to Ra of Inaba's correlation is 0.25 whereas those of

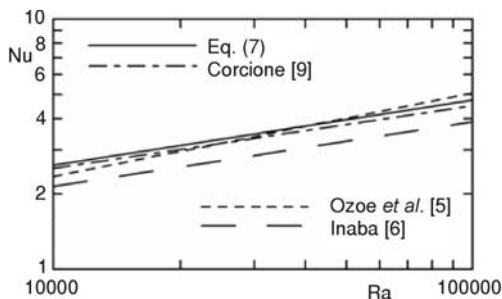


Figure 16. Comparison of Nusselt number correlations for $AR = 8$ and $\theta = 0^\circ$

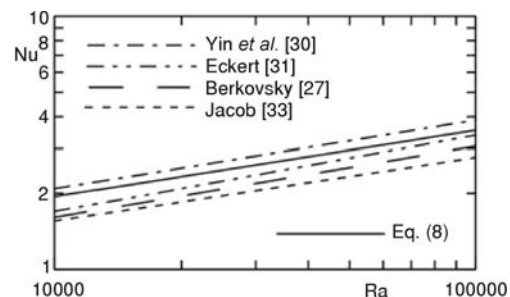


Figure 17. Comparison of Nusselt number correlations for $AR = 8$ and $\theta = 90^\circ$

Eckert and Carlson and Berkovsky and Polevikov are 0.3 and 0.28, respectively, thus these lines are not quite parallel. In this range, eq. (8) yields values 13-17% higher than those of Berkovsky and Polevikov, and 10-12% higher than Inaba's. The current correlation and that of Berkovsky and Polevikov compare better for lower aspect ratios. Although not shown in fig. 17, correlation of Newell and Schmidt [32] is 35% higher than that of Jacob's correlation [33] at $Ra = 10^5$. It is a small range of parameters that has been compared, but predictions from experiment do not agree well – fig. 17 shows that values from Yin *et al.* correlation [30] are 37 to 40% higher than those of Jacob's correlation [33] over the range $3 \cdot 10^4 \leq Ra \leq 10^5$.

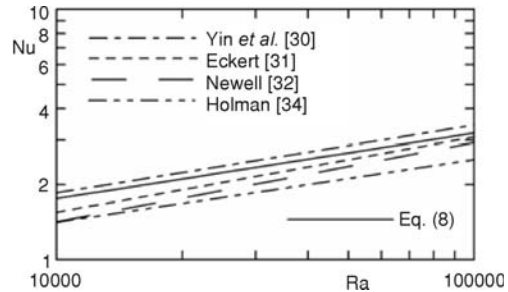


Figure 18. Comparison of Nusselt number correlations for $AR = 20$ and $\theta = 90^\circ$

In Holman's textbook [34], correlations are given for larger aspect ratio only for gas in vertical enclosure, and one of them is $\overline{Nu} = 0.197Ra^{0.25} AR^{0.111}$ for $11 \leq AR \leq 42$ and $6,000 \leq Ra \leq 2 \cdot 10^5$. This correlation is almost the same as the Jacob's correlation [33] which is based on the experimental work of Mull and Reiher [35], and the correlation constant was adjusted by Holman [34]. Holman's correlation is compared with others for $AR = 20$ in fig. 18. It should be noted that Eckert and Carlson's correlation [31] and eq. (8) in fig. 18 are out of valid correlation range. In fig. 18, Yin *et al.* correlation [30] yields values as much as 37% higher than those of Holman's correlation. El Sherbiny *et al.* [36] who performed experiments with air and perfectly conducting connecting walls show that the slope to Ra is about 0.25 up to $Ra \approx 2 \cdot 10^6$ for $AR = 5$. The slope to Ra for $AR = 10$ was about the same as $AR = 5$ in the range of $10^4 \leq Ra \leq 10^5$, but the slope becomes about 1/3 for $AR = 20$ in the same range of Ra . However, experimental results of Inaba's [6] do not show such a change in the exponent of Ra as the aspect ratio is increased from 5 to 29. The values from the correlation of El Sherbiny *et al.* [36] for $AR = 20$, which is $\overline{Nu} = [1 + (0.64Ra^{1/3})^{6.5}]^{1/6.5}$, are almost identical to Newell and Schmidt [32] in fig. 18, and thus are not plotted. Aside from the large inconsistency among correlations, a question can be raised here: which is the correct exponent to Ra for larger aspect ratio of vertical layers, such as $AR \geq 20$? In summary, there seem to be lack of detailed heat transfer studies for both horizontal and vertical layers of low aspect ratio, namely $AR < 10$. The correlations for vertical layers vary widely even for large aspect ratio studies, and there is a need for some general consensus.

Conclusions

A numerical study for 2-D natural convection in differentially heated enclosure has been performed to investigate the effect of aspect ratio and inclination angle on flow and heat transfer over the range $1 \leq AR \leq 8$, $0^\circ \leq \theta \leq 180^\circ$, and $10^3 \leq Ra \leq 10^6$. It was found that the inclination angle where the minimum heat transfer occurs has a close relationship with the flow structure transition. For small aspect ratios of 1 and 2, the secondary flow developed in the corners of enclosures was found to cause a decrease in heat transfer. For large aspect ratios of 4 and 8, a sudden decrease in heat transfer occurred as three-cell structure changed into a single cell.

The inclination angle where the maximum heat transfer occurs is larger than 50° for aspect ratios of 1 and 2, and it moves closer to 90° as Ra increases. For larger aspect ratios of 4 and 8, the maximum heat transfer occurs at 0° for all Rayleigh numbers. On the other hand, the

inclination angle where the minimum heat transfer occurs was found to increase with aspect ratio. For larger Rayleigh numbers the minimum heat transfer occurred at a lower inclination due to earlier transition from a three-cell to one-cell structure.

Correlations for average heat transfer were developed for horizontal and vertical air layers for low aspect ratios, and comparisons were made with published results. There are large inconsistencies among published results, and more studies involving some form of consensus are needed.

Nomenclature

AR	– aspect ratio ($= L/H$)	V^*	– dimensionless velocity in y-direction ($= v/(g\beta\Delta TH)^{1/2}$), [–]
H	– height of the enclosure, [m]	x, y	– cartesian co-ordinates, [m]
L	– length of the enclosure, [m]	<i>Greek symbols</i>	
Nu	– average Nusselt number ($= 1/L \int_0^L Nu_x dx$), [–]	α	– thermal diffusivity, [$m^2 s^{-1}$]
Nu_x	– local Nusselt number, [–]	β	– thermal expansion coefficient, [K^{-1}]
Ra	– Rayleigh number ($= g\beta(T_H - T_C)H^3/(v\alpha)$), [–]	ν	– kinematic viscosity, [$m^2 s^{-1}$]
T	– temperature, [K]	θ	– inclination angle, [$^\circ$]
T_0	– reference temperature ($= (T_H + T_C)/2$), [K]	<i>Subscripts</i>	
T^*	– dimensionless temperature ($= (T - T_C)/\Delta T$), [–]	H	– hot wall
U^*	– dimensionless velocity in x-direction ($= u/(g\beta\Delta TH)^{1/2}$), [–]	C	– cold wall
u	– velocity in x-direction, [ms^{-1}]		
v	– velocity in y-direction, [ms^{-1}]		

References

- [1] Dropkin, D., Somerscales, E., Heat Transfer by Natural Convection in Liquids Confined by Two Parallel Plates Which are Inclined at Various Angles with Respect to the Horizontal, *Journal of Heat Transfer*, 87 (1965), 1, pp. 77-84
- [2] Emery, A., Chu, N. C., Heat Transfer Across Vertical Layers, *Journal of Heat Transfer*, 87 (1965), 1, pp. 110-116
- [3] Eckert, E. R. G., Carlson, W. O., Natural Convection in an Air Layer Enclosed between Two Vertical Plates with Different Temperatures, *International Journal of Heat and Mass Transfer*, 2 (1961), 2, pp. 106-120
- [4] Arnold, J. N., *et al.*, Experimental Investigation of Natural Convection in Inclined Rectangular Regions of Differing Aspect Ratio, *Journal of Heat Transfer*, 98 (1976), 1, pp. 67-70
- [5] Ozoe, H., *et al.*, Natural Convection in an Inclined Rectangular Channel at Various Aspect Ratios and Angles-Experimental Measurements, *International Journal of Heat and Mass Transfer*, 18 (1975), 12, pp. 1425-1431
- [6] Inaba, H., Experimental Study of Natural Convection in an Inclined Air Layer, *International Journal of Heat and Mass Transfer*, 27 (1984), 8, pp. 1127-1139
- [7] Hamady, F. J., *et al.*, Study of Local Natural Convection Heat Transfer in a Inclined Enclosure, *International Journal of Heat and Mass Transfer*, 32 (1989), 9, pp. 1697-1708
- [8] Soong, C. Y., *et al.*, Numerical Study on Mode-Transition of Natural Convection in Differentially Heated Inclined Enclosures, *International Journal of Heat and Mass Transfer*, 39 (1996), 14, pp. 2869-2882
- [9] Corcione, M., Effects of the Thermal Boundary Conditions at the Sidewalls upon Natural Convection in Rectangular Enclosures Heated from Below and Cooled from Above, *International Journal of Thermal Sciences*, 42 (2003), 2, pp. 199-208
- [10] Wang, H., Hamed, M. S., Flow Mode-Transition of Natural Convection in Inclined Rectangular Enclosures Subjected to Bidirectional Temperature Gradients, *International Journal of Thermal Sciences*, 45 (2006), 8, pp. 782-792
- [11] Bairi, A., *et al.*, Numerical and Experimental Study of Natural Convection in Tilted Parallelepipedic Cavities for Large Rayleigh Numbers, *Experimental Thermal Fluid Science*, 31 (2007), 4, pp. 309-324

- [12] De Vahl Davis, G., Natural Convection of Air in a Square Cavity, a Bench-mark Numerical Solution, *International Journal of Numerical Methods in Fluids*, 3 (1983), 3, pp. 249-264
- [13] Tripathi, B., *et al.*, A CFD Analysis of Room Aspect Ratio on the Effect of Buoyancy and Room Air Flow, *Thermal Science*, 11 (2007), 4, pp. 79-94
- [14] Oztop, H. F., *et al.*, Laminar Natural Convection Heat Transfer in a Shed Roof with or without Eave for Summer Season, *Applied Thermal Engineering*, 27 (2007), 13, pp. 2252-2265
- [15] Biwole, P. H., *et al.*, Heat Transfer in a Double-Skin Roof Ventilated by Natural Convection in Summer Time, *Energy and Buildings*, 40 (2008), 8, pp. 1487-1497
- [16] Arici, M. E., Sahin, B., Natural Convection Heat Transfer in a Partially Divided Trapezoidal Enclosure, *Thermal Science*, 13 (2009), 4, pp. 213-220
- [17] ***, *Concentration, Heat and Momentum Limited*, Bakery House, Wimbledon Village, London, England
- [18] Spalding, D. B., *Mathematical Modelling of Fluid-Mechanics, Heat-Transfer and Chemical-Reaction Processes*, CFDU Report HTS/80/1, Imperial College, London, 1980
- [19] Van Leer, B., Towards the Ultimate Conservative Difference Scheme II, *Journal of Computational Physics*, 14 (1974), 4, pp. 361-370
- [20] Gaskell, P. H., Lau, A. K. C., Curvature-Compensated Convective Transport: SMART, a New Boundedness-Preserving Transport Algorithm, *Int. J. Numerical Methods in Fluids*, 8 (1988), 6, pp. 617-641
- [21] Barakos, G., *et al.*, Natural Convection Flow in a Square Cavity Revisited: Laminar and Turbulent Models with Wall Functions, *International Journal for Numerical Methods in Fluids*, 18 (1994), 7, pp. 695-719
- [22] Khanafer, K., *et al.*, Buoyancy-Driven Heat Transfer Enhancement in a Two-Dimensional Enclosure Utilizing Nanofluids, *International Journal of Heat and Mass Transfer*, 46 (2003), 19, pp. 3639-3653
- [23] Fusegi, T., *et al.*, A Numerical Study of Three-Dimensional Natural Convection in a Differentially Heated Cubical Enclosure, *International Journal of Heat and Mass Transfer*, 34 (1991), 6, pp. 1543-1557
- [24] Krane, R. J., Jessee, J., Some Detailed Field Measurements for a Natural Convection Flow in a Vertical Square Enclosure, *Proceedings, 1st ASME-JSME Thermal Engineering Joint Conference*, Honolulu, Hi., USA, 1983, Vol. 1, pp. 323-329
- [25] Kuypers, R. A., *et al.*, Numerical Study of Laminar and Turbulent Natural Convection in an Inclined Square Cavity, *International Journal of Heat and Mass Transfer*, 36 (1993), 11, pp. 2899-2911
- [26] Zhong, Z. Y., *et al.*, Variable Property Natural Convection in Tilted Cavities with Thermal Radiation, *Numerical Methods in Heat Transfer*, 3 (1985), pp. 195-214
- [27] Berkovsky, B. M., Polevikov, V. K., *Numerical Study of Problems on High-Intensive Free Convection, Heat Transfer and Turbulent Buoyant Convection* (Eds. D. B. Spalding, N. Afgan), Hemisphere, 1977, pp. 443-455
- [28] Mills, A. F., *Heat and Mass Transfer*, CRC Press, Boca Raton, Fla., USA, 1995
- [29] Incropera, F. P. *et al.*, *Fundamentals of Heat and Mass Transfer*, John Wiley & Sons, Hoboken, N. J., USA, 2007
- [30] Yin, S. H., *et al.*, Natural Convection in an Air Layer Enclosed within Rectangular Cavities, *International Journal of Heat and Mass Transfer*, 21 (1978), 3, pp. 307-315
- [31] Eckert, E. R. G., Carson, W. O., Natural Convection in an Air Layer Enclosed between Two Vertical Plates with Different Temperatures, *International Journal of Heat and Mass Transfer*, 2 (1961), 1-2, pp. 106-120
- [32] Newell, M.E., Schmidt, F. W., Heat Transfer by Laminar Natural Convection within Rectangular Enclosures, *Journal of Heat Transfer*, 92 (1970), 1, pp. 159-168
- [33] Jakob, M., Free Heat Convection through Enclosed Plane Gas Layers, *Journal of Heat Transfer*, 68 (1946), pp. 189-193
- [34] Holman, J. P., *Heat Transfer*, McGraw Hill, New York, N. Y., USA, 2010
- [35] Mull, W., Reiher, H., Der Warmeschutz von Luftschichten – The Heat Protection of Air Layers (in German), *Beih. Gesund. -Ing.*, 1 (1930), 28
- [36] ElSherbiny, S. M., *et al.*, Heat Transfer by Natural Convection across Vertical and Inclined Air Layers, *Journal of Heat Transfer*, 104 (1982), 1, pp. 96-102